

Review

Open Access



# Multiphase manganese-based layered oxide for sodium-ion batteries: structural change and phase transition

Zhaomeng Liu<sup>1,2</sup>, Yingying Song<sup>1,3</sup>, Shizheng Fu<sup>1</sup>, Pengyan An<sup>1</sup>, Mohan Dong<sup>1</sup>, Shuran Wang<sup>1</sup>, Qingsong Lai<sup>1</sup>, Xuan-Wen Gao<sup>1</sup>, Wen-Bin Luo<sup>1</sup> 

<sup>1</sup>Institute for Energy Electrochemistry and Urban Mines Metallurgy, School of Metallurgy, Northeastern University, Shenyang 110819, Liaoning, China.

<sup>2</sup>Key Laboratory of Advanced Energy Materials Chemistry (Ministry of Education), Nankai University, Tianjin 300071, China.

<sup>3</sup>School of Science and Engineering, University of Dundee, Nethergate, Dundee, Scotland DDI 4HN, UK.

**Correspondence to:** Dr. Wen-Bin Luo, Institute for Energy Electrochemistry and Urban Mines Metallurgy, School of Metallurgy, Northeastern University, Wenhua Road, Heping District, Shenyang 110819, Liaoning, China. E-mail: luowenbin@smm.neu.edu.cn

**How to cite this article:** Liu Z, Song Y, Fu S, An P, Dong M, Wang S, Lai Q, Gao XW, Luo WB. Multiphase manganese-based layered oxide for sodium-ion batteries: structural change and phase transition. *Microstructures* 2024;4:2024036. <https://dx.doi.org/10.20517/microstructures.2024.01>

**Received:** 8 Jan 2024 **First Decision:** 19 Mar 2024 **Revised:** 9 Apr 2024 **Accepted:** 22 May 2024 **Published:** 12 Jun 2024

**Academic Editor:** Shaobo Cheng **Copy Editor:** Fangling Lan **Production Editor:** Fangling Lan

## Abstract

Sodium-ion batteries (SIBs) are recognized as a leading option for energy storage systems, attributed to their environmental friendliness, natural abundance of sodium, and uncomplicated design. Cathode materials are crucial in defining the structural integrity and functional efficacy of SIBs. Recent studies have extensively focused on manganese (Mn)-based layered oxides, primarily due to their substantial specific capacity, cost-effectiveness, non-toxic nature, and ecological compatibility. Additionally, these materials offer a versatile voltage range and diverse configurational possibilities. However, the complex phase transition during a circular process affects its electrochemical performance. Herein, we set the multiphase Mn-based layered oxides as the research target and take the relationship between the structure and phase transition of these materials as the starting point, aiming to clarify the mechanism between the microstructure and phase transition of multiphase layered oxides. Meanwhile, the structure-activity relationship between structural changes and electrochemical performance of Mn-based layered oxides is revealed. Various modification methods for multiphase Mn-based layered oxides are summarized. As a result, a reasonable structural design is proposed for producing high-performance SIBs based on these oxides.

**Keywords:** Sodium-ion batteries, cathode, Mn-based layered oxides, structural change, phase transition



© The Author(s) 2024. **Open Access** This article is licensed under a Creative Commons Attribution 4.0 International License (<https://creativecommons.org/licenses/by/4.0/>), which permits unrestricted use, sharing, adaptation, distribution and reproduction in any medium or format, for any purpose, even commercially, as long as you give appropriate credit to the original author(s) and the source, provide a link to the Creative Commons license, and indicate if changes were made.



## INTRODUCTION

Energy is the foundation of human survival and development<sup>[1-3]</sup>. Nevertheless, as the economy has rapidly developed, energy shortages, pollution, and other issues have increased in prominence<sup>[4-6]</sup>. In recent years, clean and renewable energy has been the focus of research<sup>[7-10]</sup>. Electrochemical energy storage devices have also seen an increase in demand year after year, and energy storage systems, including secondary batteries, have received wide attention<sup>[11-13]</sup>. Currently, lithium secondary batteries have found widespread application in various domains, including portable electronic gadgets, electric vehicles, and numerous other sectors<sup>[14-16]</sup>. Nevertheless, the heightened demand for lithium resources, coupled with the uneven geographical distribution of lithium mines and the complexities associated with extraction, have spurred growing interest in alternative energy storage technologies<sup>[17-21]</sup>. Sodium-ion batteries (SIBs) are anticipated to facilitate substantial energy storage solutions, primarily because of their economical nature and the plentiful availability of sodium resources<sup>[22-26]</sup>. Being a critical element of SIBs, the cathode material significantly influences their specific capacities, energy densities, power densities, and overall lifespan<sup>[27-30]</sup>. However, due to the large size of Na<sup>+</sup> (1.02 Å) embedded in/out of the electrode structure, the material will produce irreversible volume and structural deformation, resulting in capacity decay, limiting the development of SIBs<sup>[31-34]</sup>. Therefore, it is crucial to develop a stable cathode material.

Within the scope of cathode materials, transition metal (TM) layered oxides, symbolized as Na<sub>x</sub>MO<sub>2</sub> (where M stands for a TM), have emerged as the most significant for SIBs. This prominence is attributed to the periodic layered architecture, straightforward synthesis methodology, and high specific capacity and voltage capabilities<sup>[35-38]</sup>. Manganese (Mn) is the most abundant raw material on earth; Na<sub>x</sub>MO<sub>2</sub> and its derivatives synthesized from Mn as the TM have been widely studied<sup>[39-42]</sup>. Mn-based oxides mainly include the tunnel-type, spinel-type, and layered oxides. The common synthesis methods of manganese oxides include the solid phase, coprecipitation, sol-gel, and spray drying techniques<sup>[43]</sup>. Based on the coordination configuration of sodium ions in TMO<sub>6</sub> (TM = Ni, Co, Mn, Fe) polyhedral and the stacking mode of oxygen, sodium-manganese layered oxides (NMLOs) can be divided into four main categories: O3, O2, P3, P2, etc. Nonetheless, Mn<sup>3+</sup> is prone to the Jahn-Teller effect. High spin Mn<sup>3+</sup> in MnO<sub>6</sub> octahedral units in the materials leads to serious lattice distortion, which usually has a serious adverse influence on structural stability and electrochemical performance<sup>[44]</sup>. According to the coordination configuration of Na<sup>+</sup> and the stacking mode of oxygen, Na<sub>x</sub>MnO<sub>2</sub> exists mainly in O3-type and P2-type structures<sup>[45-48]</sup>. O3 and P2 structural materials have their own advantages<sup>[49-51]</sup>. Specifically, there is only one occupation of sodium ions in O3-type Mn-based oxides. Therefore, the initial sodium content of O3 phase material is higher than that of P2 phase material, and the capacity is larger<sup>[52-54]</sup>. While the interlayer spacing of P2-type structure is larger, the P2-type Mn-based layered material has a wider sodium ion transport channel<sup>[36]</sup>. Na<sup>+</sup> can diffuse directly between two adjacent triangular prism sites through this channel. Therefore, P2-type Mn-based layered cathode materials can exhibit a high rate capability<sup>[55]</sup>. O3-type and P2-type materials both suffer problems such as the Jahn-Teller effect, dissolution of transition manganese, complex phase transition of crystal structure and air stability.

In order to study the mechanism of manganese oxides, *in-situ* X-ray diffraction (XRD) and synchrotron radiation X-ray absorption spectroscopy can effectively monitor the structural and valence changes and dig out the phase transition mechanism of the Mn-based oxides. The intricate phase transition observed in Na<sub>x</sub>MO<sub>2</sub> materials plays a pivotal role in influencing the electrochemical efficacy of SIBs<sup>[56]</sup>. In the process of Na<sup>+</sup> intercalation/de-intercalation, the O3 phase is accompanied by a complex phase transition (multiple platforms)<sup>[57]</sup>. The phase transition process alters the volumetric dimensions of the material's structure, leading to distortion and disintegration of the layered configuration, which, in turn, impacts the cyclic stability of the battery<sup>[58]</sup>. Upon charging P2-type structures with reduced sodium levels to high voltages, the

sodium concentration within the crystal lattice becomes insufficient. This deficiency diminishes the shielding effect of  $\text{Na}^+$  ions on oxygen atoms. Consequently, the increased electrostatic repulsion among neighboring oxygen atoms facilitates the slippage of adjacent TM layers, leading to a phase transition from the P2-type to the O2-type<sup>[59-61]</sup>. The phase transition will lead to excessive volume changes, showing severe capacity decay in fewer cycles<sup>[62-64]</sup>. However, compared with traditional single-phase Mn-based cathode materials, the multiphase materials can withstand great stress due to their special mixed structure, and multiphase is conducive to the rapid migration of sodium ions owing to the existence of phase with large interlayer spacing<sup>[65,66]</sup>. Multiphase Mn-based layered materials can integrate the characteristics of different structures and achieve multi-functional advantages in order to obtain better electrochemical performance. Therefore, it is significant to summarize and anticipate the potential of these multiphase materials<sup>[67-69]</sup>. At the same time, in the construction of composite structures, a number of strategies have been proven to be effective, including adjusting ion substitution, surface coating, and some other strategies such as controlling sodium content and calcination temperature<sup>[70-72]</sup>.

In this review, we consolidate the findings on the structural characteristics and phase transitions of multiphase Mn-based layered oxide materials utilized in SIBs. Additionally, we delve into their evolution, structural tuning, interface alterations, and various other modification techniques [Figure 1]. By comprehensively examining the development status of multiphase Mn-based layered materials, we reveal the phase transition process of multiphase structures and clarify different modification strategies to obtain a stable circular process. Furthermore, we have proposed several recommendations and outlooks regarding the future advancement of Mn-based layered oxide materials as cathodic components in SIBs.

## DEVELOPMENT OF MULTIPHASE MN-BASED LAYERED MATERIALS

Currently, various O3 or P2 phase Mn-based layered materials, both single and multiple, have been reported as cathodes for SIBs, which have shown good performance. However, there are still deficiencies in terms of capacity, stability, and power. For this reason, a comprehensive structural advantage strategy combining O3 and P2 phases was proposed in order to enhance electrochemical performance. As shown in Figure 2A, Guo *et al.* first proposed a Mn-based layered material that combines both P2 and O3 phases<sup>[73]</sup>. Thereinto, the layered oxides with P2 and O3 composite structures were clearly characterized at atomic resolution. The two-phase synergy of the P2 + O3 layered material can provide high reversible capacity, and it still has a high capacity retention after 150 times sodium intercalation/de-intercalation. This proves the feasibility of multiphase Mn-based layered materials. As shown in Figure 2B, Qi *et al.* reported  $\text{Na}_{0.78}\text{Ni}_{0.2}\text{Fe}_{0.38}\text{Mn}_{0.42}\text{O}_2$  cathode material with both O3 and P2 hybrid phases for SIBs<sup>[74]</sup>. This material owns the advantages of both P2 and O3 structures, demonstrates a reversible capacity of  $86 \text{ mAh g}^{-1}$ , and exhibits outstanding rate and cycling performance. Even at an elevated current rate of 10 C, it retains 66% of its initial capacity. Notably, after 1,500 cycles, the capacity retention rate stands at 90%. In addition, *in-situ* XRD was performed in varying voltage ranges to examine structural changes during electrochemical testing. The findings indicate that an upper voltage limit of 4 V is ideal, resulting in reduced polarization, enhanced structural integrity, and improved cyclic stability. These outcomes offer valuable insights for devising the most appropriate structure and mitigating phase transitions in layered cathode materials. As shown in Figure 2C, Zhou *et al.* reported that a mixed P2/O3 phase structure  $\text{Na}_{0.67}\text{Fe}_{0.5}\text{Mn}_{0.46}\text{Mg}_{0.04}\text{O}_2$  cathode is prepared and achieves excellent electrochemical performances<sup>[75]</sup>. Because of the synergistic effect of P2 and O3,  $\text{Na}^+$  ions can achieve an extremely high ion diffusion rate in a battery. Simultaneously, it has been demonstrated that binary TM oxide materials comprising Fe and Mn possess significant potential for use as cathode materials for SIBs. Nonetheless, the limited cycling stability of Fe/Mn layered oxide cathodes remains a primary obstacle. As shown in Figure 2D, Zhang *et al.* successfully synthesized P2/O3 two-phase  $\text{Na}_{0.67}\text{Fe}_{0.425}\text{Mn}_{0.425}\text{Cu}_{0.15}\text{O}_2$  layered oxides using the sol-gel method<sup>[76]</sup>.

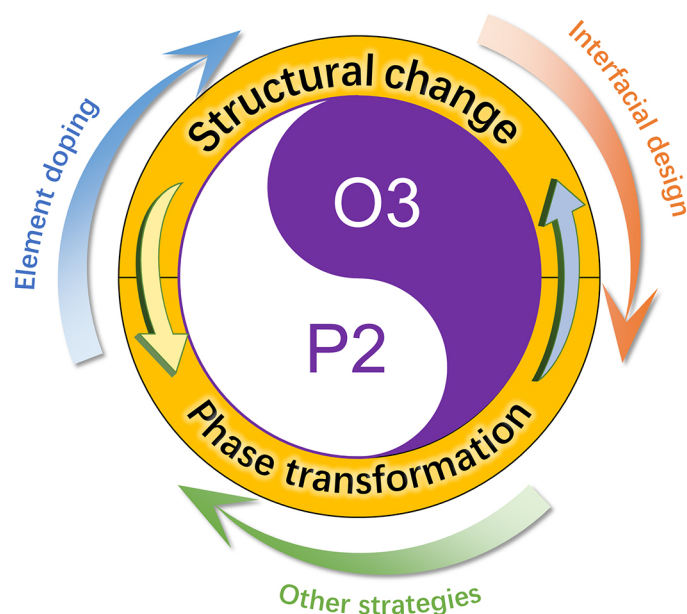


**Figure 1.** Schematic illustration of multiphase Mn-based layered oxide for sodium-ion batteries: structural change and phase transition.

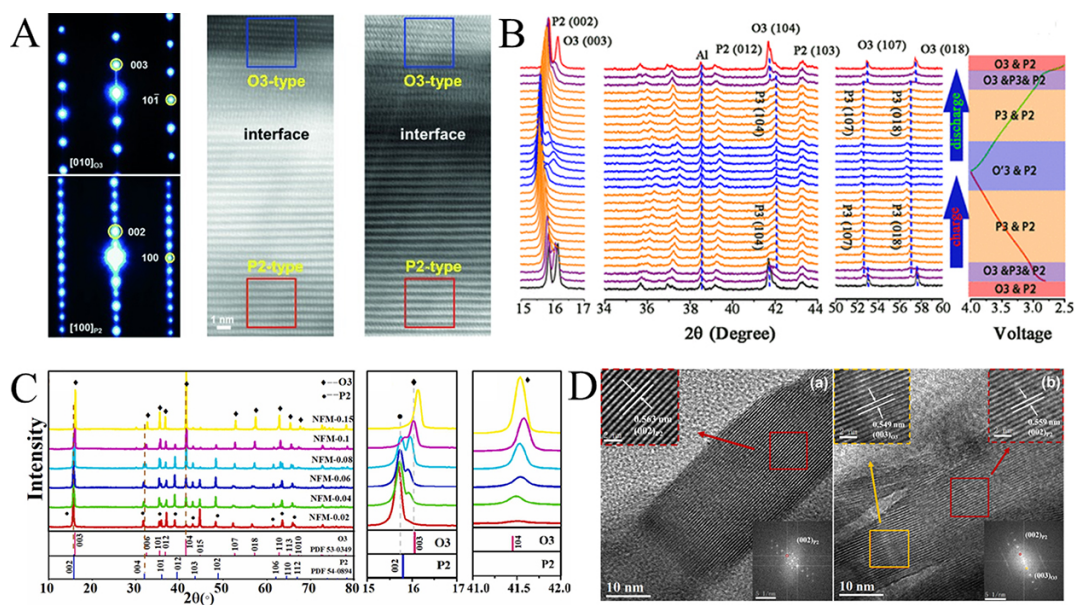


**Figure 2.** (A) The SAED patterns of the P2 + O3 NaLiMNC composite: O3-type structure and P2-type structure; The STEM images: HADDF and ADF images of P2 + O3 NaLiMNC composite; the blue and red rectangle represent O3 structure and P2 structure areas (Reproduced with permission from Ref. [73]. Copyright 2015, John Wiley and Sons); (B) *In-situ* XRD patterns collected during the first charge/discharge of NNFM-0.78 cell under 0.1 Cover a voltage range of 2.5-4.0 V, with the corresponding electrochemical charge-discharge profile (Reproduced with permission from Ref. [74]. Copyright 2017, American Chemical Society); (C) XRD patterns of NFM-0.02, NFM-0.04, NFM-0.06, NFM-0.08, NFM-0.1, NFM-0.15, the magnification of 15°-17°, the magnification of 41°-42° (Reproduced with permission from Ref. [75]. Copyright 2023, Elsevier); (D) Cycling performance of NFM-0.02, NFM-0.04, NFM-0.06, NFM-0.08, NFM-0.1, NFM-0.15 (Reproduced with permission from Ref. [76]. Copyright 2024, Elsevier).

The substitution of copper (Cu) is noted to facilitate the transformation of the P2 phase to the O3 phase. By fine-tuning the quantity of Cu, a P2/O3 composite structure is achievable. Furthermore, due to the synergetic effect of the composite phase and Cu substitution, *in-situ* XRD analyses reveal that this

composite configuration, comprising P2 and O3 phases, enables highly reversible phase transitions and minimizes lattice discrepancies during Na<sup>+</sup> ion insertion/extraction. After cycling 100 times at a rate of 1 C, the dual-phase Na<sub>0.67</sub>Fe<sub>0.425</sub>Mn<sub>0.425</sub>Cu<sub>0.15</sub>O<sub>2</sub> cathode exhibits a capacity retention of 87.1%. In contrast, the single-phase P2-Na<sub>0.67</sub>Fe<sub>0.425</sub>Mn<sub>0.425</sub>Cu<sub>0.15</sub>O<sub>2</sub> electrode shows a capacity retention of only 36.4%. Consequently, the dual-phase structures are confirmed as an effective approach to implement high-performing Fe/Mn-based layered oxide cathodes.

In addition to the Fe/Mn system, comprehensive studies have been conducted on multi-component P2/O3 dual-phase materials, primarily focusing on Mn-based components. As depicted in [Figure 3A](#), Zhang *et al.* have synthesized a multi-component P2/O3 dual-phase material Na<sub>0.732</sub>Ni<sub>0.273</sub>Mg<sub>0.096</sub>Mn<sub>0.63</sub>O<sub>2</sub> comprising 78.39% P2 phase Na<sub>0.67</sub>Ni<sub>0.33</sub>Mn<sub>0.67</sub>O<sub>2</sub> and 21.61% O3 phase NaNi<sub>0.5</sub>Mn<sub>0.5</sub>O<sub>2</sub><sup>[66]</sup>. Although possessing identical elemental compositions, the two phases show distinct crystal structures. Structural assessments and density functional theory (DFT) calculations reveal that the composite material tends to form an atomic-level symbiotic structure. The intricate lattice configuration of the dual-phase structure acts as a barrier against undesirable ion and oxygen movement during electrode processes. As a result, this dual-phase framework notably enhances electrochemical performance while preserving exceptional reversibility in anionic oxygen redox reactions. Moreover, the coexistence of heteroepitaxial structures in P2 and O3 phases creates multiphase boundaries, which lead to an interlocking effect due to their differing electrochemical behaviors. This phenomenon helps prevent significant structural degradation and reduces the lattice strain associated with Na<sup>+</sup> deintercalation and intercalation. As a result, the co-existing P2/O3 composites demonstrate increased capacity and cycle performance and reversible structural evolution. As presented in [Figure 3B](#), Wang *et al.* have documented the creation and detailed analysis of a new P2/O3 intercalated Na<sub>0.8</sub>Mn<sub>y</sub>Ni<sub>0.8-y</sub>Fe<sub>0.1</sub>Ti<sub>0.1</sub>O<sub>2</sub> (where *y* values are 0.6, 0.55, 0.5, 0.45) quaternary cathode material<sup>[77]</sup>. Electrochemical evaluations reveal that the P2/O3 dual-phase materials exhibit superior performance in SIBs compared to single P2 or O3 phases, confirming the advantageous impact of the co-growth of P2 and O3 materials. Transmission electron microscopy was utilized to investigate the interface properties of P2/O3. The studies indicate the formation of a semi-coherent interface along the *a/b* and *c* axes, with a localized variation in the concentration of TMs at the interface of the two phases. Energy Dispersive X-ray Detector (EDX) and Electron Energy Loss Spectroscopy (EELS) analyses elucidate a charge compensation mechanism that hinges on the alteration in the distribution of transition elements. This mechanism facilitates equilibrium between differing sodium concentrations in P2 and O3 phases. The above data offers an enhanced comprehension of P2/O3 dual-phase materials. Relative to the initial cathode composition, the optimized P2/O3-Na<sub>0.8</sub>Mn<sub>0.55</sub>Ni<sub>0.25</sub>Fe<sub>0.1</sub>Ti<sub>0.1</sub>O<sub>2</sub> cathode, achieved through the fine-tuning of Mn and Ni ratios, demonstrates superior rate capability and augmented energy density.

Hong *et al.* successfully synthesized P2/O3 dual-phase cathode Na<sub>0.73</sub>Ni<sub>0.4</sub>Mn<sub>0.4</sub>Ti<sub>0.2</sub>O<sub>2</sub> using the solid-phase method by mixing P2 and O3, and the content of P2 phase was 33%<sup>[78]</sup>. Based on the results from XRD refinement, it was observed that the interlayer spacing along the *c*-axis in the pure P2 material decreased from 5.6055 to 5.5710 Å in the dual-phase P2 phase. Conversely, the interlayer spacing in the pure O3 material expanded from 5.4502 to 5.4855 Å in the dual-phase O3 phase. This indicates varying electrostatic repulsion among the TM oxide layers in these two phases. Compared with the singular P2 or O3 phase, the dual-phase cathode exhibits a high initial Coulombic efficiency near 100%, with enhanced specific discharge capacity and average voltage. As illustrated in [Figure 3C](#), Xu *et al.* analyzed the sodium ion deintercalation process in sodium-containing layered metal oxides Na<sub>x</sub>TMO<sub>2</sub> (TM = Ni, Cu, Fe, Mn) within both the P2 and O3 phases with electrochemical collision method. Their findings highlight distinct electrochemical behaviors between the two materials<sup>[79]</sup>. In O3-type oxides, the likelihood of Na<sup>+</sup> diffusion within a single particle is higher than that in P2-type oxides. This observation contradicts the conventional belief that P2-

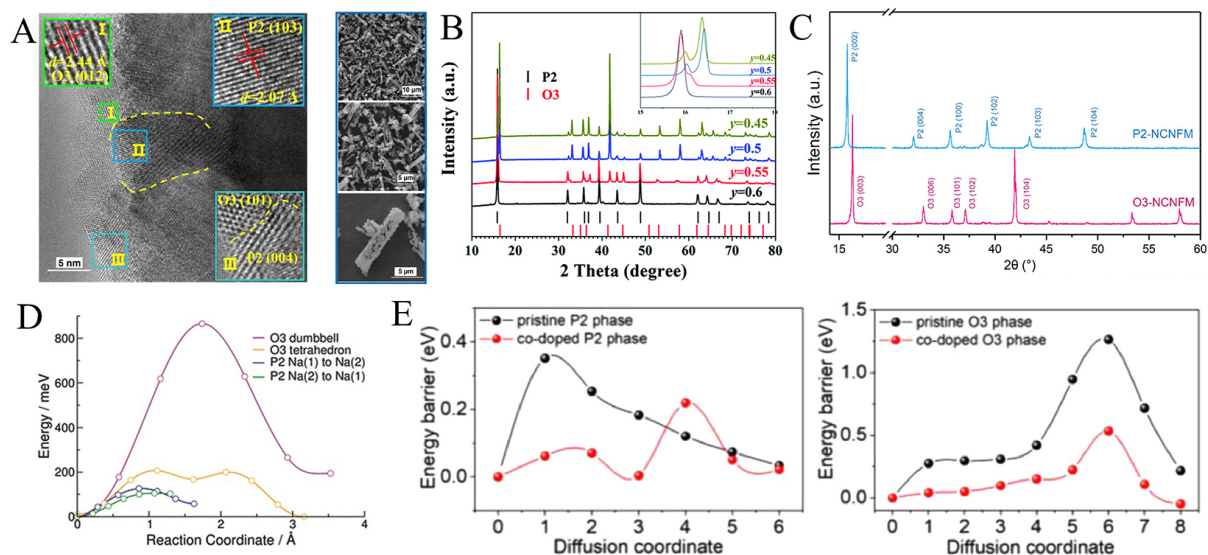


**Figure 3.** (A) TEM images of P2/O3-Co<sub>950</sub> 0.8 materials with the insert of SEAD image and partly enlarged graphic and SEM images of P2/O3-Co<sub>950</sub> 0.8 materials (Reproduced with permission from Ref. [66]. Copyright 2024, Elsevier); (B) XRD patterns of Na<sub>0.8</sub>Mn<sub>y</sub>Ni<sub>0.8-y</sub>Fe<sub>0.1</sub>Ti<sub>0.1</sub>O<sub>2</sub> (y = 0.6, 0.55, 0.5, 0.45) with the inset showing a magnified range (from 15° to 18°) corresponding to the (002) and (003) peaks of the P2 and O3 structures, respectively (Reproduced with permission from Ref. [77]. Copyright 2024, Elsevier); (C) XRD profiles of as-prepared layered oxides: P2-NCNFM and O3-NCNFM (Reproduced with permission from Ref. [79]. Copyright 2024, Elsevier); (D) The lines connecting the points in correspond to a spline fitted to the calculated CI-NEB energies (Reproduced with permission from Ref. [55]. Copyright 2024, John Wiley and Sons); (E) The corresponding migration energy barriers for Na-ion diffusion using NEB calculations (Reproduced with permission from Ref. [80]. Copyright 2024, Elsevier).

type cathodes generally offer greater Na<sup>+</sup> conductivity than their O3 counterparts. As demonstrated, dual-phase and multiphase cathodes are exceedingly advantageous for high-energy SIBs despite the structural phase transitions during cycling being considerably intricate. For the stabilization of multiphase materials, it is imperative to strategically design their morphology and structure to enhance their electrochemical characteristics. Figure 3D shows the computed energy profiles for the sodium ion diffusion paths discussed above [55]. The dumbbell hop in the O3 phase shows a large activation energy,  $E_a = 866$  meV. In contrast, tetrahedral hops require much less energy barriers,  $E_a = 201$  meV, and the energy profile shows a local minimum at 168 meV above the ground state, corresponding to the Na atom located in a high-energy tetrahedral site. The corresponding computed migration energy barriers for sodium-ion diffusion are shown in Figure 3E [80]. There is no huge difference on energy barriers for sodium-ion migration between pristine P2-Na<sub>0.7</sub>MnO<sub>2</sub> and doped P2-Na<sub>0.7</sub>MnO<sub>2</sub>, which is attributed to their similar crystal parameters. However, the energy barriers for sodium-ion migrations in doped O3-NaMn<sub>0.5</sub>Ni<sub>0.5</sub>O<sub>2</sub> (0.04-0.53 eV) are much lower than that of pristine O3-NaMn<sub>0.5</sub>Ni<sub>0.5</sub>O<sub>2</sub> (0.21-1.26 eV). The significant decrease of energy barriers in doped O3-NaMn<sub>0.5</sub>Ni<sub>0.5</sub>O<sub>2</sub> can be attributed to the expansion of parameter *c* and Na interlayer. From the theoretical calculation result, it is obvious that the volume of the P2 phase changes little during the ion insertion process, which proves that its structure is stable, while the O3 phase shows the expansion of parameter *c* during the cycle process, which proves poor structural stability.

## MODIFIED METHODS

### Elemental doping

Element substitution can induce a synergistic interaction between phases, consequently stabilizing dual-phase materials and augmenting their electrochemical attributes. To enhance electrochemical performance, various cations, such as Li<sup>+</sup>, Mg<sup>2+</sup>, Cu<sup>2+</sup>, Al<sup>3+</sup>, Ti<sup>4+</sup>, and others, are employed to substitute the Mn element in the base material. This substitution modifies physical properties, including the internal configuration of the

layered oxide crystal structure, to boost electrochemical efficiency. Thus, element substitution emerges as a viable approach for manipulating the phase composition of  $\text{Na}_x\text{MnO}_2$  layered oxides. As a notable example of layered oxide cathodes for SIBs, P2-type Na-FeMn layered oxide (NFMO) achieves high specific discharge capacity but suffers from limited cycling stability, whereas O3-type NFMO offers prolonged cycle life yet at a reduced capacity. To leverage the electrochemical complementarity of these two phases, a unique P2/O3 dual-phase structure of  $\text{Na}_{0.67}\text{Li}_{0.11}\text{Fe}_{0.36}\text{Mn}_{0.36}\text{Ti}_{0.17}\text{O}_2$  was synthesized through a substantial Li/Ti co-substitution strategy. The substitution of Li at the Mn site in P2/O3- $\text{Na}_{0.67}\text{Li}_{0.11}\text{Fe}_{0.36}\text{Mn}_{0.36}\text{Ti}_{0.17}\text{O}_2$  led to a cathode exhibiting enhanced cycle stability between 2.0 and 4.2 V, as illustrated in [Figure 4A](#)<sup>[81]</sup>. The enhancement in performance is attributed to the structural transformation from P2 to P2/O3 type induced by Li substitution. A high degree of Li substitution in the TM layer, below 4.2 V, facilitates reversible oxygen redox due to the creation of an oxygen-bonding environment. This results in an unprecedented capacity of 235 mAh g<sup>-1</sup>, the highest recorded for all Fe and Mn-based layered oxide cathodes. The distinct and intricate intersecting pattern at the phase boundary effectively suppresses the transition from the P2 to OP4 phase.

The substitution also lessens the lattice mismatch between the two phases at elevated potential. While Ti substitution maintains the phase structure intact, it forms a robust Mn-O-Ti-O-Fe bond within the TM layer, bolstering structural stability. However, this comes at the cost of reduced capacity due to electrochemical inactivity of Ti. The research revealed that the effects of Li doping are largely contingent on the site of substitution: Lithium ions occupying the TM site preserve the P2 phase, and during charging, they can migrate to the Na layer, acting as a pillar to fortify cycle stability. Conversely, a substantial introduction of Li<sup>+</sup> ions typically leads to a transformation from the P2-type to a more structurally stable O3-type configuration. However, given that Li<sup>+</sup> ions are electrochemically inactive, excessive Li substitution can diminish the specific capacity of batteries. Utilizing Li-substituted  $\text{Na}_x\text{Li}_{1-x}\text{Mn}_{0.66}\text{Ni}_{0.17}\text{Co}_{0.17}\text{O}_2$  (with  $0.50 \leq x \leq 0.80$ ) as a foundation, Huang *et al.* synthesized a series of P3/P2/O'3 layered composite materials<sup>[82]</sup>. [Figure 4B](#) illustrates that aberration-corrected scanning transmission electron microscopy and X-ray analysis have confirmed the coherence of the nanostructured composite material existing within the layered composite. The three-phase composite material, P3/P2/O'3, exhibits significantly improved specific capacity and cycle performance compared to the original material. As depicted in [Figure 4C](#), Yu *et al.* achieved a thermodynamically stable P2/O3 dual-phase structure in  $\text{Na}_{0.85}\text{Ni}_{0.34}\text{Mn}_{0.66-x}\text{Ti}_x\text{O}_2$  by modulating the Ti substitution level. This approach effectively suppressed the emergence of the O2 phase under high-pressure conditions and facilitated a fully reversible structural evolution when subjected to a high pressure of 4.4 V<sup>[83]</sup>.

[Figure 4D](#) demonstrates that the fabricated dual-phase structure mitigates structural strain and significant changes in lattice volume, thereby enhancing its structural robustness under high-pressure conditions. Hu *et al.* synthesized  $\text{Na}_{0.8}\text{Li}_{0.27}\text{Mn}_{0.68}\text{Ti}_{0.05}\text{O}_2$ , a cathode material featuring a P2/O3 coexistent structure, achieved through Ti substitution at the Mn site<sup>[84]</sup>. The dual-phase composite structure, augmented by substituting inactive elements, notably benefits from the synergistic effect. Ti substitution mitigates the Mn<sup>3+</sup>/Mn<sup>4+</sup> redox reaction and enhances the stability of oxygen charge compensation. From a structural evolution standpoint, Ti substitution curbs Li<sup>+</sup> loss and prevents irreversible structural degradation throughout the cycling process. It improves the oxygen redox capacity of the material by increasing electron density around oxygen ions without compromising the reversibility of oxygen redox reactions. The P2/O3 electrode demonstrates a high initial charge-discharge capacity and exceptional cycling performance. In [Figure 4E](#), Gao *et al.* introduced a novel mixed P2 + T phase  $\text{Na}_x\text{Co}_{0.1}\text{Mn}_{0.9}\text{O}_2$  design, wherein Co doping in  $\text{Na}_x\text{MnO}_2$  addresses the Jahn-Teller distortion associated with Mn (III)<sup>[85]</sup>. The phase interfaces between P2-type and T-type materials create extra pathways and active sites, facilitating rapid Na<sup>+</sup> transport and enhanced charge storage, leading to increased electronic and ionic conductivity. The synthesized material

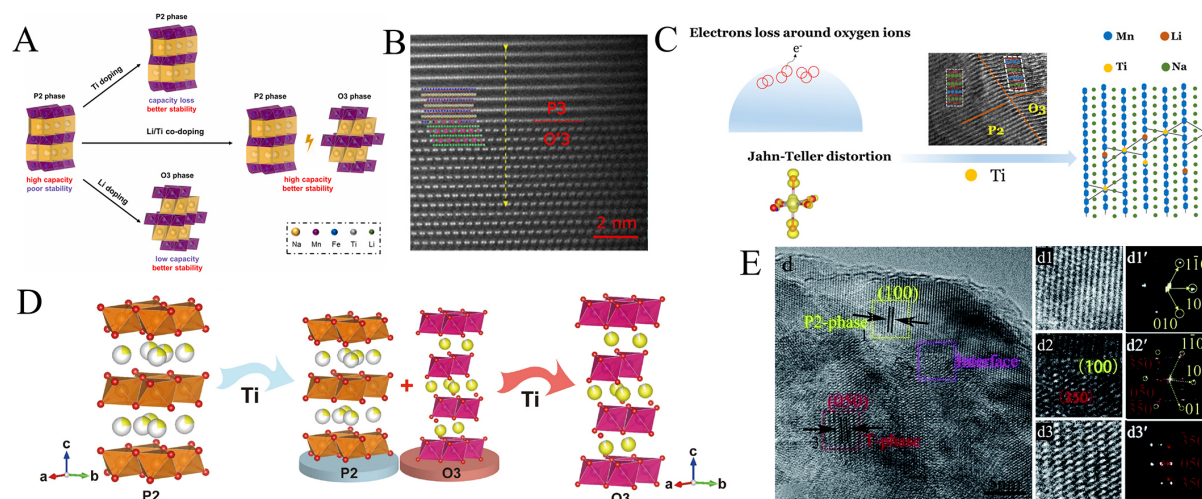


**Figure 4.** (A) Schematic illustration of the design of the P2/O3 biphasic structure for sodium Fe/Mn-based layered oxide cathode (Reproduced with permission from Ref.<sup>[81]</sup>. Copyright 2021, Elsevier); (B) HAADF-STEM image of the P3/O3 composite (Reproduced with permission from Ref.<sup>[82]</sup>. Copyright 2018, Elsevier); (C) Graphic abstract of the Deciphering the Origin of High Electrochemical Performance in a Novel Ti-Substituted P2/O3 Biphasic Cathode for Sodium-Ion Batteries (Reproduced with permission from Ref.<sup>[83]</sup>. Copyright 2022, Elsevier); (D) Schematic illustration of phase transition process with increasing Ti content (Reproduced with permission from Ref.<sup>[84]</sup>. Copyright 2020, American Chemical Society); (E) HRTEM images of the P2 + T material. The amplified figure of the rectangular region (d1-d3) and the corresponding Fast Fourier Transform (FFT) diffraction (d1'-d3') (Reproduced with permission from Ref.<sup>[85]</sup>. Copyright 2018, Royal Society of Chemistry).

displays exceptional performance, achieving a high specific discharge capacity of 219 mAh g<sup>-1</sup> at 0.1 C and a sodium storage capacity of 117 mAh g<sup>-1</sup> at 5 C. These results surpass those of the most advanced Na<sub>x</sub>MnO<sub>2</sub> systems.

Through high-temperature calcination, as shown in Figure 5A, Zhang *et al.* doped Cu elements into Na[Mn<sub>0.6</sub>Fe<sub>0.4</sub>]O<sub>2</sub> to synthesize O3 dual-phase layered oxides. By adjusting the amount of Cu<sup>2+</sup> doping, P2-NaMn<sub>0.6</sub>Fe<sub>0.4</sub>O<sub>2</sub> was induced to transform into the O3 phase<sup>[86]</sup>. The refined dual-phase NaMn<sub>0.48</sub>Fe<sub>0.32</sub>Cu<sub>0.2</sub>O<sub>2</sub> demonstrates a remarkable Na<sup>+</sup> diffusion coefficient and superior sodium storage capabilities. It achieves an impressive capacity retention rate of 82.9% after 100 cycles, with a specific discharge capacity of 103.76 mAh g<sup>-1</sup>. In Figure 5B, Feng *et al.* have developed a series of P2/O3 dual-phase Na<sub>0.80</sub>Li<sub>0.13</sub>Ni<sub>0.20</sub>Fe<sub>x</sub>Mn<sub>0.67-x</sub>O<sub>2</sub> (x = 0, 0.05, 0.10, 0.15) materials, accomplished by substituting a portion of Mn with Fe<sup>[87]</sup>. In addition to its air stability, this material exhibits high capacity and cycling stability. It delivers a reversible specific capacity of 172.02 mAh g<sup>-1</sup>, with a capacity retention rate of 88.60% after 100 cycles at a 1 C rate. The occurrence of irreversible phase transitions can considerably diminish the cycle life. Typically, under high pressures, the irreversible phase transition from P2 to O2 occurs within a 4 V range. As illustrated in Figure 5C, Wang *et al.* employed partial Mg substitution for Ni to synthesize Na<sub>0.67</sub>Mn<sub>0.67</sub>Ni<sub>0.28</sub>Mg<sub>0.05</sub>O<sub>2</sub>. This approach effectively prevents the P2 to O2 phase transformation under high pressure, thereby enhancing structural stability<sup>[88]</sup>. Figure 5D presents the work of Wang *et al.* who synthesized Mg-substituted Na<sub>0.6</sub>[Mn<sub>0.6</sub>Ni<sub>0.4-x</sub>Mg<sub>x</sub>]O<sub>2</sub>. They discovered that the TM layer in this composition induces “Na-O-Mg” and “Mg-O-Mg” phase transitions within the layered structure<sup>[89]</sup>. Tao *et al.* modified the layered oxide Na<sub>0.67</sub>Ni<sub>0.33</sub>Mn<sub>0.67</sub>O<sub>2</sub> through Ti substitution<sup>[90]</sup>. This resulted in a reversible capacity of 89.6 mAh g<sup>-1</sup> at the current density of 5 C, coupled with outstanding cycling performance, maintaining 88.78% capacity retention after 200 cycles at current density of 0.5 C. Element doping and substitution have been established as efficacious strategies for crystal structure stabilization and enhancement of electrochemical performance of materials. However, single-element doping might not always yield effective

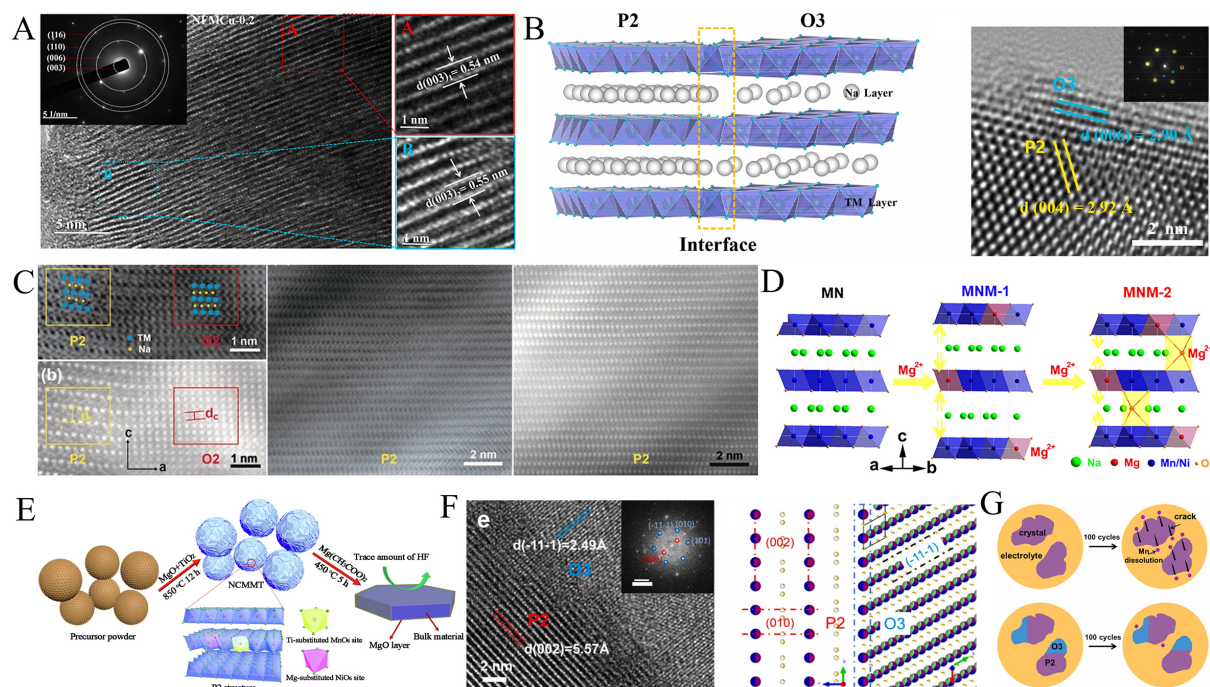


**Figure 5.** (A) Large area HR-TEM image showing the atomic structure of the selected grain (inset SADE pattern). The two regions denoted with A and B have different local crystallographic orientation (Reproduced with permission from Ref.<sup>[86]</sup>. Copyright 2019, John Wiley and Sons); (B) The schematic diagram of two-phase interface and the HRTEM of Fe<sub>0.10</sub>-LNM (Reproduced with permission from Ref.<sup>[87]</sup>. Copyright 2019, John Wiley and Sons); (C) ABF- and HAADF-STEM images of a P2-type Na<sub>0.67</sub>Mn<sub>0.67</sub>Ni<sub>0.33-x</sub>Mg<sub>x</sub>O<sub>2</sub> ( $x = 0$ ) electrode when charging to 4.22 V at the [010] zone axis; The yellow and red rectangles indicate areas with the P2 and O2 structure; ABF- and HAADF-STEM images of a P2-type Na<sub>0.67</sub>Mn<sub>0.67</sub>Ni<sub>0.33-x</sub>Mg<sub>x</sub>O<sub>2</sub> ( $x = 0.05$ ) electrode when charging to 4.22 V (Reproduced with permission from Ref.<sup>[88]</sup>. Copyright 2016, John Wiley and Sons); (D) Structural evolution of MNM-x with Mg substitution (Reproduced with permission from Ref.<sup>[89]</sup>. Copyright 2019, John Wiley and Sons); (E) Schematic illustration of M-NCMMT (Reproduced with permission from Ref.<sup>[91]</sup>. Copyright 2022, Elsevier); (F) HRTEM image at the phase boundary of NLFMTO. Inset is the corresponding FFT map. Red and blue circles are used to mark the reflection spots for P2 and O3 phases, respectively. The scale bar in the FFT map is 5.1 nm. Structure illustration to show the unique intersected complex way at the phase boundary between P2 and O3 phases for NLFMTO (Reproduced with permission from Ref.<sup>[81]</sup>. Copyright 2016, John Wiley and Sons). (G) Schematic illustration of the structural changes for P2-type NFMO and P2/O3 biphasic NLFMTO after long-term cycling (Reproduced with permission from Ref.<sup>[81]</sup>. Copyright 2018, American Chemical Society).

results, leading to explorations in double or multi-element doping. As illustrated in Figure 5E, Wang *et al.* employed a dual modification approach, encompassing Mg/Ti co-doping and magnesium oxide (MgO) surface coating, to address the shortcomings of P2-type Na<sub>0.67</sub>Ni<sub>0.17</sub>Co<sub>0.17</sub>Mn<sub>0.66</sub>O<sub>2</sub> cathodes<sup>[91]</sup>. The findings reveal that Mg/Ti co-substitution solidifies the P2 structure, and the MgO layer effectively shields against HF corrosion on the surface while facilitating Na<sup>+</sup> migration. Moreover, the electrochemical performance of the modified Na<sub>0.67</sub>Ni<sub>0.17</sub>Co<sub>0.17</sub>Mn<sub>0.66</sub>Mg<sub>0.1</sub>O<sub>2</sub> surpasses that of the unmodified material, with a high 111.6 mAh g<sup>-1</sup> initial discharge capacity, retaining 90.6% at 100 mA g<sup>-1</sup> ranging from 2 to 4.5 V, significantly outperforming Na<sub>0.67</sub>Ni<sub>0.17</sub>Co<sub>0.17</sub>Mn<sub>0.76</sub>O<sub>2</sub>. Figure 5F presents a Fe/Mg/Li co-substitution method to further refine the electrochemical performance of P2-type Na<sub>2/3</sub>Ni<sub>1/3</sub>Mn<sub>2/3</sub>O<sub>2</sub> materials. This approach incorporates electroactive Fe to reduce Mn content, while the addition of electrochemically inactive Mg disrupts in-plane ordering, thereby strengthening structural stability<sup>[81]</sup>. Figure 5G presents that low-valent Li not only bolsters the structural robustness of the layered oxide cathode material through Mn oxidation state elevation via charge compensation but also increases its Na content, thereby amplifying its reversible capacity<sup>[81]</sup>.

### Coating two phases

Beyond element doping, the manipulation of interfaces is pivotal for the electrochemical characteristics of materials. Mn-based layered TM oxides often undergo several detrimental alterations, including (i) dissolution of manganese and other active TMs; (ii) surface degradation due to acidic substance erosion in the electrolyte; (iii) a thick Cathode Electrolyte Interface (CEI) layer on the electrode surface after repetitive cycles; (iv) extensive electrolyte consumption; and (v) impediment of Na diffusion. The most straightforward and effective solution to these issues is coating a protective layer on the electrode surface. This coating prevents the direct interaction between the active material and the electrolyte, mitigates acid effects such as HF, and decelerates electrolyte decomposition. Surface coating has been confirmed as a potent method for enhancing the electrochemical performance of SIBs. It achieves this by introducing an artificial second-phase solid electrolyte interface (SEI) film on the electrode while preserving the integrity of the electronic conductive network. To facilitate interface engineering and enhance the electrochemical behavior of layered oxide cathode materials in SIBs, various metal oxides and phosphate coatings (such as  $\text{Al}_2\text{O}_3$ ,  $\text{CuO}$ , and  $\text{ZrO}_2$ ) are employed.

As demonstrated in [Figure 6A](#), Kaliyappan *et al.* employed atomic layer deposition technology for applying varying thicknesses of  $\text{Al}_2\text{O}_3$  on  $\text{P2-Na}_{2/3}(\text{Mn}_{0.54}\text{Ni}_{0.13}\text{Co}_{0.13})\text{O}_2$ <sup>[92]</sup>. This alteration improved electrochemical performance, with the material discharging  $123 \text{ mAh g}^{-1}$  at a current density of 1C and surpassing the original material in cycle stability. Liu *et al.*, as seen in [Figure 6B](#), highlighted that a thin  $\text{Al}_2\text{O}_3$  surface coating can effectively curb adverse reactions at high voltages<sup>[93]</sup>. While oxide materials offer solid protection against electrolyte erosion and boost cycle stability, they are generally non-conductive to  $\text{Na}^+$  and do not facilitate  $\text{Na}^+$  diffusion or charge transfer at interfaces. Hence, an ideal coating material should not only protect the electrode but also facilitate sodium ion diffusion through a three-dimensional path, ensuring superior rate performance.

As demonstrated in [Figure 6C](#), Li *et al.* *in-situ* coated  $\text{O3-NaNi}_{1/3}\text{Mn}_{1/3}\text{Fe}_{1/3}\text{O}_2$  with sodium ion conductor  $\text{Na}_2\text{SiO}_3$ , effectively preventing phase transitions<sup>[94]</sup>. This  $\text{Na}_2\text{SiO}_3$  coating reduces polarization, mitigates voltage drop, and supports a larger  $\text{Na}^+$  diffusion coefficient with its three-dimensional sodium ion diffusion path. As presented in [Figure 6D](#), Xue *et al.* applied a  $\text{ZnO}$  coating to P2-type  $\text{Na}_{2/3}[\text{Ni}_{1/3}\text{Mn}_{2/3}]\text{O}_2$  cathode material using a simple wet chemical method<sup>[95]</sup>.  $\text{ZnO}$  serves as a barrier against electrolyte corrosion and particle detachment, enhancing  $\text{Na}^+$  kinetics during the extraction and insertion processes due to the improved electrode-electrolyte interface.  $\text{Zn}^{2+}$  replaces the TM layer, shortens the metal-oxygen bond length, and reinforces the material's structural stability, collectively boosting the electrochemical performance of  $\text{Na}_{2/3}[\text{Ni}_{1/3}\text{Mn}_{2/3}]\text{O}_2$ , with the  $\text{ZnO}$ -coated cathode showing robust capacity retention.

As displayed in [Figure 6E](#), Hwang *et al.* enhanced the cycle performance of  $\text{Na}_{0.67}\text{Ni}_{0.33}\text{Mn}_{0.67}\text{O}_2$  cathode material by coating it with  $\text{MgO}$ <sup>[96]</sup>. They successfully applied varying thicknesses of  $\text{MgO}$ , which exhibited very low charge transfer resistance. At a rate of  $0.2 \text{ }^\circ\text{C}$  and in the voltage range of 2.0-4.5 V, the initial reversible discharge capacity reached  $105 \text{ mAh g}^{-1}$ , with a cycle retention rate as high as 81.5%. Hwang *et al.* synthesized  $\text{Al}_2\text{O}_3$  nanoparticle-coated  $\text{O3-Na}[\text{Ni}_{0.6}\text{Co}_{0.2}\text{Mn}_{0.2}]\text{O}_2$  cathodes using a simple dry ball milling method, effectively reducing parasitic reactions in the electrolyte solution and enhancing  $\text{Na}^+$  migration. The modified material reveals a specific capacity of  $151 \text{ mAh g}^{-1}$  and outstanding cycle stability and rate capability.

[Figure 7A](#) illustrates Yong-Mook Kang's synthesis of layered oxide cathodes with multiple phases, whose characteristics shift based on the sodium ion content, significantly influencing their electrochemical performance<sup>[97]</sup>. The nonstoichiometric nature of these layered oxides with sodium ions affects not only

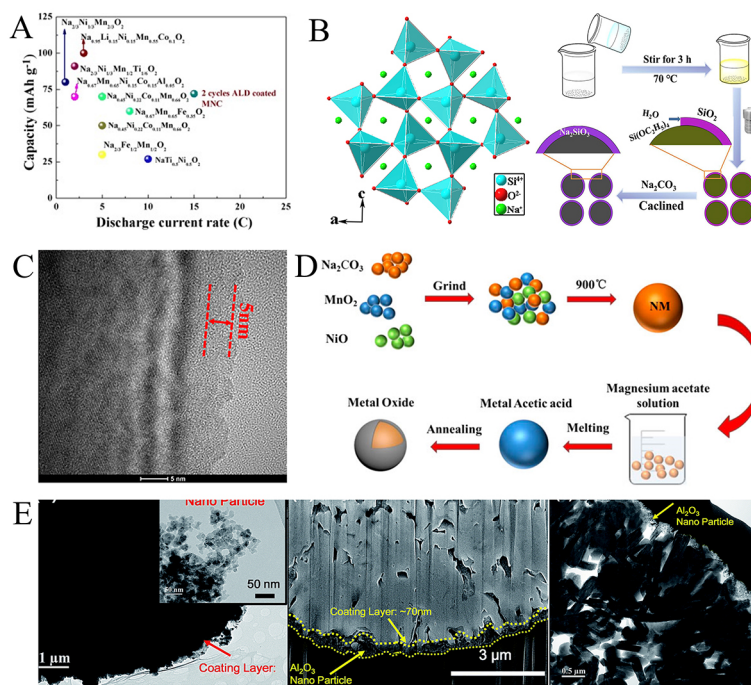


**Figure 6.** (A) Electrochemical performance between  $\text{Na}_{2/3}(\text{Mn}_{0.54}\text{Ni}_{0.13}\text{Co}_{0.13})\text{O}_2$  and other cathode materials for sodium-ion batteries (Reproduced with permission from Ref. [92]. Copyright 2019, Elsevier); (B) The structure of  $\text{Na}_2\text{SiO}_3$ ; Schematic illustration of the synthesis process for  $\text{Na}_2\text{SiO}_3@\text{NaNi}_{1/3}\text{Mn}_{1/3}\text{Fe}_{1/3}\text{O}_2$  (Reproduced with permission from Ref. [93]. Copyright 2019, John Wiley and Sons); (C) HRTEM images of NNMMO@ZnO sample (Reproduced with permission from Ref. [94]. Copyright 2019, Elsevier); (D) Schematic diagram of MgO-coated NM cathodes (Reproduced with permission from Ref. [95]. Copyright 2022, Frontiers); (E) Microscopic analysis of the  $\text{Al}_2\text{O}_3$  coated  $\text{Na}[\text{Ni}_{0.6}\text{Co}_{0.2}\text{Mn}_{0.2}]\text{O}_2$  particle: bright field TEM image (inset image: TEM image of  $\text{Al}_2\text{O}_3$  nanoparticles), cross-sectional SEM image, and cross-sectional TEM image (Reproduced with permission from Ref. [96]. Copyright 2013, Royal Society of Chemistry).

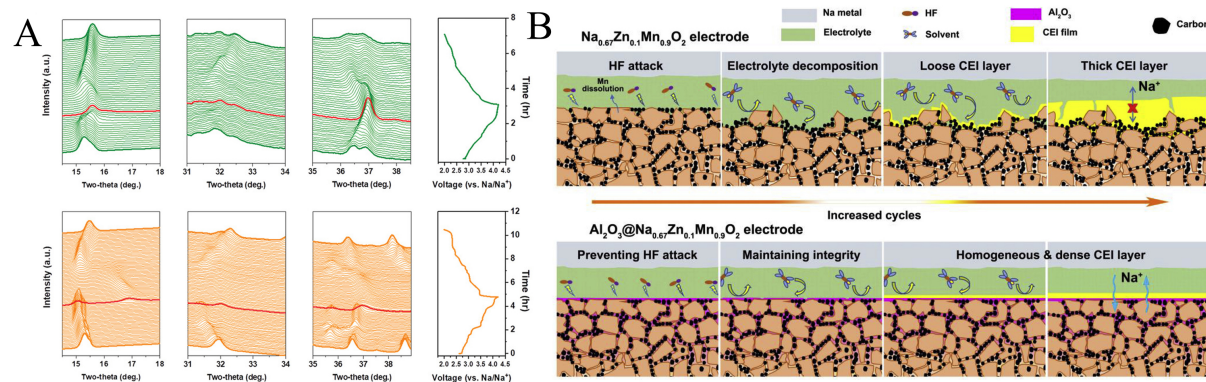


**Figure 7.** (A) *In-situ* XRD patterns and corresponding charge/discharge curves of 1st cycle measured at a C-rate of 0.25 C of pristine NMO and activated NMO (Reproduced with permission from Ref. [97]. Copyright 2021, John Wiley and Sons); (B) Schematic illustration of the surficial evolutions of  $\text{Na}_{0.67}\text{Zn}_{0.1}\text{Mn}_{0.9}\text{O}_2$  and  $\text{Al}_2\text{O}_3@\text{Na}_{0.67}\text{Zn}_{0.1}\text{Mn}_{0.9}\text{O}_2$  electrodes (Reproduced with permission from Ref. [98]. Copyright 2020, Elsevier).

their capacity but also their cycle stability and kinetics, underscoring the critical role of sodium ion content. However,  $\text{Na}_2\text{CO}_3$  is prone to irreversible formation on the surface due to the loss of sodium ions from the lattice, leading to detrimental effects when the stoichiometric Na-containing O3 phase transitions to a non-stoichiometric P2 phase. Addressing this issue involves decomposing  $\text{Na}_2\text{CO}_3$  into electrochemically active

sodium ions while transforming the non-stoichiometric P2 phase back to a stoichiometric O3. The study emphasizes that minimizing sodium ion loss and maintaining a lattice structure rich in sodium ions are crucial for achieving electrochemical benefits in developing sodium-containing layered cathodes.

Element doping and surface engineering can synergistically enhance the structural stability of materials in some cases. As depicted in [Figure 7B](#), Zuo *et al.* engineered an  $\text{Al}_2\text{O}_3@\text{Na}_{0.67}\text{Zn}_{0.1}\text{Mn}_{0.9}\text{O}_2$  coating through  $\text{Zn}^{2+}$  substitution and  $\text{Al}_2\text{O}_3$  atomic layer deposition. This design capitalizes on the benefits of structural stability and surface passivation to mitigate related challenges<sup>[98]</sup>. Additionally, the uniform and resilient CEI layer formed on the  $\text{Al}_2\text{O}_3$ -coated electrode effectively blocks further decomposition of the organic electrolyte, enhancing the material's overall performance.

### Other strategies

Sodium layered oxides often exhibit instability in deep desorption within the P2 structure and sluggish kinetics in the O3 structure. Hence, developing dual-phase materials that merge the benefits of both P2 and O3 structures is advantageous. Beyond the previously discussed strategies of element substitution and surface coating, additional methods exist for fabricating two-phase layered oxide materials. [Figure 8A](#) shows that Xiao *et al.* precisely manipulated structural evolution and created high-performance heterostructured dual-phase layered oxide cathodes through local chemical and orbital hybridization modulation. They employed macroscopic and atomic-scale techniques to vividly depict the layered P2 and O3-type heterostructures<sup>[99]</sup>. Owing to the synergistic advantages of symbiotic structure and local environment adjustment, local chemical modulation is utilized to foster energy and crystal structure evolution, forming layered symbiotic oxide cathodes.

[Figure 8B](#) highlights that Zhou *et al.* put forward  $\text{Na}_{0.7}\text{Mn}_{0.4}\text{Ni}_{0.3}\text{Cu}_{0.1}\text{Fe}_{0.1}\text{Ti}_{0.1}\text{O}_{1.95}\text{F}_{0.1}$  with a P2/O3 dual-phase structure as a novel high-entropy cathode material<sup>[80]</sup>. This composition integrates various elemental benefits, with Mn and Ni elements as primary redox species, Fe element mitigating the Jahn-Teller effect of Mn, Cu element enhancing  $\text{Na}^+$  mobility and air stability, Ti element preventing phase transitions, and F element inducing cation redistribution. The formation of the P2/O3 dual phase during synthesis was examined through high-temperature *in situ* XRD and electron microscopy. As shown in [Figure 8C](#), Jiang *et al.* crafted Co-substituted  $\text{Na}_x\text{MnO}_2$  nanosheets with an adjustable P2/P3 dual-phase structure<sup>[100]</sup>. The optimized P2/P3- $\text{Na}_{0.67}\text{Mn}_{0.64}\text{Co}_{0.30}\text{Al}_{0.06}\text{O}_2$  cathode delivers impressive rate performance and cycle stability due to the unique P2/P3 dual phase with a stable crystal structure and rapid  $\text{Na}^+$  diffusion. The structural evolution during the  $\text{Na}^+$  extraction/insertion process was investigated using operational XRD, effectively curbing the P2-P2' phase transition. [Figure 8D](#) presents Zhu *et al.*'s design of a stable layered P2@P3 mixed-phase integrated spinel  $\text{Na}_{0.5}\text{Ni}_{0.1}\text{Co}_{0.15}\text{Mn}_{0.65}\text{Mg}_{0.1}\text{O}_2$  cathode material<sup>[61]</sup>. This cathode, with dual functional advantages, demonstrates high reversible specific capacity, excellent rate performance, and cycle stability. Guo *et al.*, using co-precipitation and subsequent solid-state reaction, achieved the integration of O3 and lithium-substituted P2 hosts in the P2 + O3 layered oxide complex ( $\text{Na}_{0.66}\text{Li}_{0.18}\text{Mn}_{0.71}\text{Ni}_{0.21}\text{Co}_{0.08}\text{O}_2$ ). This biphasic synergy between the P2 and O3 complex is well established during the electrochemical reaction process, showcasing a substantial discharge capacity at a rate of 0.1 C<sup>[73]</sup>.

## RESULTS AND PROSPECTS

The development of advanced characterization techniques has led to a growing understanding of layered oxide materials for SIBs. From synthesis methods to structural changes, the subtle changes of this promising cathode material during charge and discharge are revealed. However, sodium ion layered oxides still have limitations. For this reason, the design of two or more non-interacting phases will produce electrodes with intermediate phases but excellent properties, and further, multiphase materials can provide better

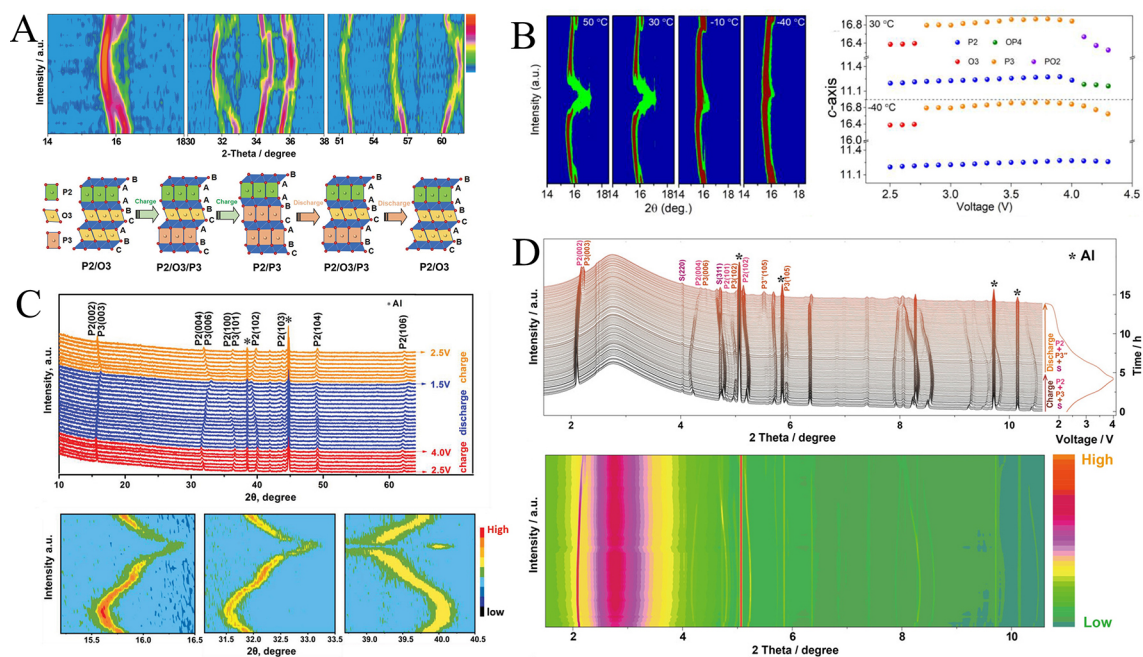


**Figure 8.** (A) Intensity contour maps (bird's eye view) showing the evolution of the main characteristic diffraction peaks; Schematic illustration of the crystal structural evolution during the cycling (Reproduced with permission from Ref. [99]. Copyright 2022, John Wiley and Sons); (B) Contour plots of *in-situ* XRD patterns at various temperatures, and evolution of lattice parameters upon Na<sup>+</sup> extraction (Reproduced with permission from Ref. [80]. Copyright 2023, Elsevier); (C) Operando XRD patterns during the charge/discharge process in the voltage range of 1.5-4 V (vs. Na<sup>+</sup>/Na). Black asterisks represent peaks from Al window; Corresponding intensity contour maps (bird's eye view) concerning the evolution of the main characteristic diffraction peaks (Reproduced with permission from Ref. [100]. Copyright 2021, John Wiley and Sons); (D) *In-situ* synchrotron-based XRD patterns collected during the first cycle at 0.1 C, with the corresponding charge/discharge curve on the right; Intensity contour map and corresponding three-dimensional (3D) maps (Reproduced with permission from Ref. [61]. Copyright 2020, John Wiley and Sons).

performance than expected from simple mixtures. It is necessary to investigate the recent phase transition of layered oxide two-phase materials in the sodium ion insertion and deinsertion reaction. Exploring the core mechanisms underlying the evolution of layered dual-phase cathode materials during their charging and discharging cycles continues to be a crucial area for future research. Delving into these mechanisms is challenging, yet the amalgamation of advanced characterization techniques, offering higher precision and real-time micro-level observation, brings us closer to understanding the most authentic reaction processes. The emergence of various sophisticated *in-situ* characterization methods, such as *in-situ* X-ray, optical, and electron imaging technologies, forms a vital foundation for the detailed examination of these micro-mechanisms.

Currently, research on dual-phase cathode materials, particularly those enhanced through surface coating and elemental doping, has achieved significant strides in numerous aspects. Although element doping can improve the structural stability of the material, it will lose part of its capacity. Coating two phases can effectively improve the side reaction between the electrode and the electrolyte interface, inhibiting the Jahn-teller effect, but achieving a complete and uniform coating has become a research difficulty. Large-scale preparation of other modification schemes has not been fully achieved. Hence, it is important to recognize that a singular approach often addresses only specific issues and brings about limited enhancements, thereby falling short of fulfilling multiple simultaneous requirements. For real-world applications, cathode materials need to surmount a range of challenges. Consequently, a holistic approach that integrates and applies various modification techniques is necessary to address these challenges comprehensively and

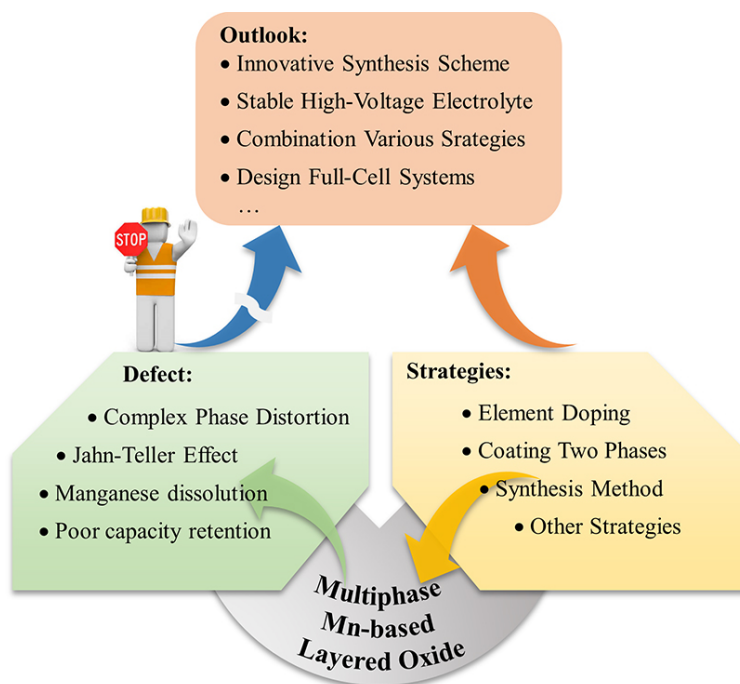


**Figure 9.** Summary of the negative effects, suppression strategies, and prospects for future high-performance SIBs in multiphase manganese-based layered oxides.

enhance the overall efficacy of layered oxide cathode materials for SIBs. Based on the existing research, the multiphase Mn-based layered oxide cathode materials for SIBs can be further optimized from the following ideas in the future [Figure 9].

Firstly, solid-phase, ball milling, sol-gel, and hydrothermal methods can be used to synthesize multiphase Mn-based layered oxides, but their large-scale production remains challenging. Hence, developing suitable and effective synthesis schemes is the premise of designing and constructing high-performance multiphase Mn-based layered oxide materials. A suitable synthesis scheme can prevent the  $\text{H}_2\text{O}/\text{CO}_2$  in the atmospheric environment from being easily embedded into the interlayer during the synthesis, resulting in structural damage and improving electrochemical performance. At the same time, the appropriate scheme can also improve the sodium deficiency state of the multiphase Mn-based layered oxide, which can increase the energy density and promote the sodium storage ability and commercial value of Mn-based layered TM oxide cathodes.

In addition, it is necessary to develop a stable high-voltage electrolyte for multiphase Mn-based layered oxides. For most layered TM oxide cathodes, the theoretical operating voltage window can usually reach over 4.0 V. However, carbonate ester-based electrolytes usually undergo severe decomposition in the high-pressure range. Therefore, to obtain high energy density, the development of stable high-voltage electrolytes is the key to realizing the high energy density advantage of SIBs. The formation and characteristics of the SEI on the anode and the positive electrolyte interface (CEI) on the cathode play an important role in the design and matching of SIBs. Therefore, developing functional additives to improve the performance of the electrolyte and promote the formation of a stable CEI film on the electrode will become a research hotspot and a difficulty.

Furthermore, a single strategy usually only solves specific problems and achieves limited improvement, making it difficult to meet multiple needs. For practical applications, cathode materials face diverse challenges. The organic combination of various modification methods and the integration of their respective advantages is the general trend in future research and development of layered oxide cathodes. As more advanced characterization methods are developed, we can better understand the reaction mechanism and structure-activity relationship of materials. They are also vital to achieving greater breakthroughs in the field of layered oxide cathodes. Therefore, a comprehensive application and integration strategy of various modification methods should be developed to solve multiple problems and improve the overall performance of multiphase Mn-based layered oxide cathode materials for SIBs.

Finally, despite the rapid development of layered oxide cathodes for SIBs, most current research of multiphase Mn-based layered oxides is based on the performance and mechanism tests of half-cell systems. Sodium reacts at high voltage, forming a thick and unstable surface layer. As a reference electrode, it is highly dependent on the electrolyte and atmospheric composition, which produces an unstable potential and leads to an inaccurate evaluation of the cathode material. This seriously affects rate and voltage measurements. Therefore, to realize the practical application of SIBs, it is necessary to find a reference electrode with stable static potential and chemical inertness that works stably in the electrochemical window with the most commonly used electrolyte to achieve a comprehensive evaluation of layered oxide batteries' performance and finally achieve high-performance sodium ion full battery devices.

## **DECLARATIONS**

### **Authors' Contributions**

Developed the concept: Luo WB, Liu Z

Conducted the frame of the paper: Lai Q, Gao XW

Gathered the initial characterizations and data analysis: Liu Z, Song Y

Collected the various works of literature: An P, Dong M, Wang S

Written the manuscript, helped to polish this paper: Fu S, Luo WB

All authors discussed the results and commented on the manuscript.

### **Availability of Data and Materials**

Not applicable.

### **Financial support and sponsorship**

The work was financially supported by the National Natural Science Foundation of China (No. 52204308 and No. 52272194), the LiaoNing Revitalization Talents Program (Grant No. XLYC2007155), the Natural Science Foundation of Liaoning Province (2023-MSBA-101), the Postdoctoral Science Foundation of China (No. ZX20220158), and the Postdoctoral Foundation of Northeastern University.

### **Conflicts of interest**

All authors declared that there are no conflicts of interest.

### **Ethical approval and consent to participate**

Not applicable.

### **Consent for publication**

Not applicable.

## Copyright

© The Author(s) 2024.

## REFERENCES

1. Harper G, Sommerville R, Kendrick E, et al. Recycling lithium-ion batteries from electric vehicles. *Nature* 2019;575:75-86. DOI
2. Liu H, Zhu Z, Yan Q, et al. A disordered rock salt anode for fast-charging lithium-ion batteries. *Nature* 2020;585:63-7. DOI
3. Zhou Y, Su M, Yu X, et al. Real-time mass spectrometric characterization of the solid-electrolyte interphase of a lithium-ion battery. *Nat Nanotechnol* 2020;15:224-30. DOI
4. Wang J, Fan L, Liu Z, et al. In situ alloying strategy for exceptional potassium ion batteries. *ACS Nano* 2019;13:3703-13. DOI
5. Ge J, Fan L, Wang J, et al. MoSe<sub>2</sub>/N-doped carbon as anodes for potassium-ion batteries. *Adv Energy Mater* 2018;8:1801477. DOI
6. Mu J, Zhao Z, Gao X, et al. Bimetallic PdFe<sub>3</sub> nano-alloy with tunable electron configuration for boosting electrochemical nitrogen fixation. *Adv Energy Mater* 2023;14:2303558. DOI
7. Zhang Q, Wang L, Wang J, et al. Low-temperature synthesis of edge-rich graphene paper for high-performance aluminum batteries. *Energy Stor Mater* 2018;15:361-7. DOI
8. Zhao L, Gao X, Gu Q, et al. Realizing a dendrite-free metallic-potassium anode using reactive prewetting chemistry. *eScience* 2024;4:100201. DOI
9. Hu Z, Hao J, Shen D, et al. Electro-spraying/spinning: a novel battery manufacturing technology. *Green Energy Environ* 2024;9:81-8. DOI
10. Yu W, Ge J, Hu Y, et al. Hybrid high-performance aqueous batteries with potassium-based cathode||zinc metal anode. *Sci China Mater* 2023;66:923-31. DOI
11. Wang J, Wang B, Lu B. Nature of novel 2D van der Waals heterostructures for superior potassium ion batteries. *Adv Energy Mater* 2020;10:2000884. DOI
12. Li L, Liu L, Hu Z, et al. Understanding high-rate K<sup>+</sup>-solvent co-intercalation in natural graphite for potassium-ion batteries. *Angew Chem Int Ed* 2020;59:12917-24. DOI
13. Wang L, Menakath A, Han F, et al. Identifying the components of the solid-electrolyte interphase in Li-ion batteries. *Nat Chem* 2019;11:789-96. DOI
14. Mackanic DG, Yan X, Zhang Q, et al. Decoupling of mechanical properties and ionic conductivity in supramolecular lithium ion conductors. *Nat Commun* 2019;10:5384. DOI PubMed PMC
15. Manthiram A. A reflection on lithium-ion battery cathode chemistry. *Nat Commun* 2020;11:1550. DOI PubMed PMC
16. Wang J, Zhang G, Liu Z, et al. Li<sub>3</sub>V(MoO<sub>4</sub>)<sub>3</sub> as a novel electrode material with good lithium storage properties and improved initial coulombic efficiency. *Nano Energy* 2018;44:272-8. DOI
17. Liu Z, Wang J, Ding H, Chen S, Yu X, Lu B. Carbon nanoscrolls for aluminum battery. *ACS Nano* 2018;12:8456-66. DOI
18. Liu Z, Wang J, Jia X, et al. Graphene armored with a crystal carbon shell for ultrahigh-performance potassium ion batteries and aluminum batteries. *ACS Nano* 2019;13:10631-42. DOI
19. Zhao L, Gao X, Mu J, et al. Durable integrated K-metal anode with enhanced mass transport through potassiphilic porous interconnected mediator. *Adv Funct Mater* 2023;33:2304292. DOI
20. Liu Z, Wang J, Lu B. Plum pudding model inspired KVPO<sub>4</sub>F@3DC as high-voltage and hyperstable cathode for potassium ion batteries. *Sci Bull* 2020;65:1242-51. DOI
21. Guo YJ, Wang PF, Niu YB, et al. Boron-doped sodium layered oxide for reversible oxygen redox reaction in Na-ion battery cathodes. *Nat Commun* 2021;12:5267. DOI PubMed PMC
22. Ji H, Ji W, Xue H, et al. Synergistic activation of anionic redox via cosubstitution to construct high-capacity layered oxide cathode materials for sodium-ion batteries. *Sci Bull* 2023;68:65-76. DOI
23. Huang Z, Zhang X, Zhao X, et al. Hollow Na<sub>0.62</sub>K<sub>0.05</sub>Mn<sub>0.7</sub>Ni<sub>0.2</sub>Co<sub>0.1</sub>O<sub>2</sub> polyhedra with exposed stable {001} facets and K riveting for sodium-ion batteries. *Sci China Mater* 2023;66:79-87. DOI
24. Liu Q, Hu Z, Chen M, et al. Recent progress of layered transition metal oxide cathodes for sodium-ion batteries. *Small* 2019;15:e1805381. DOI
25. Shi Q, Qi R, Feng X, et al. Niobium-doped layered cathode material for high-power and low-temperature sodium-ion batteries. *Nat Commun* 2022;13:3205. DOI PubMed PMC
26. Wang C, Liu L, Zhao S, et al. Tuning local chemistry of P2 layered-oxide cathode for high energy and long cycles of sodium-ion battery. *Nat Commun* 2021;12:2256. DOI PubMed PMC
27. Wang F, Zhang J, Lu H, et al. Production of gas-releasing electrolyte-replenishing Ah-scale zinc metal pouch cells with aqueous gel electrolyte. *Nat Commun* 2023;14:4211. DOI PubMed PMC
28. Xu GL, Liu X, Zhou X, et al. Native lattice strain induced structural earthquake in sodium layered oxide cathodes. *Nat Commun* 2022;13:436. DOI PubMed PMC
29. Deng T, Ji X, Zou L, et al. Interfacial-engineering-enabled practical low-temperature sodium metal battery. *Nat Nanotechnol* 2022;17:269-77. DOI
30. Zhao Y, Kang Y, Wozny J, et al. Recycling of sodium-ion batteries. *Nat Rev Mater* 2023;8:623-34. DOI
31. Zuo W, Innocenti A, Zarrabeitia M, Bresser D, Yang Y, Passerini S. Layered oxide cathodes for sodium-ion batteries: storage

- mechanism, electrochemistry, and techno-economics. *ACC Chem Res* 2023;56:284-96. DOI PubMed PMC
32. Cao X, Li H, Qiao Y, et al. Stabilizing reversible oxygen redox chemistry in layered oxides for sodium-ion batteries. *Adv Energy Mater* 2020;10:1903785. DOI
  33. Hu Z, Geng C, Wang L, Lv W, Yang Q. Revisiting the roles of carbon in the catalysis of lithium-sulfur batteries. *Adv Energy Sustain Res* 2024;5:2300148. DOI
  34. Xiao Y, Abbasi NM, Zhu Y, et al. Layered oxide cathodes promoted by structure modulation technology for sodium-ion batteries. *Adv Funct Mater* 2020;30:2001334. DOI
  35. Hu HY, Wang H, Zhu YF, et al. A universal strategy based on bridging microstructure engineering and local electronic structure manipulation for high-performance sodium layered oxide cathodes. *ACS Nano* 2023;17:15871-82. DOI
  36. Liu S, Wan J, Ou M, et al. Regulating Na occupation in P2-type layered oxide cathode for all-climate sodium-ion batteries. *Adv Energy Mater* 2023;13:2203521. DOI
  37. Shen L, Wang Y, Lv H, et al. Ultrathin  $Ti_2Nb_2O_9$  nanosheets with pseudocapacitive properties as superior anode for sodium-ion batteries. *Adv Mater* 2018;30:e1804378. DOI
  38. Chu S, Kim D, Choi G, et al. Revealing the origin of transition-metal migration in layered sodium-ion battery cathodes: random Na extraction and Na-free layer formation. *Angew Chem Int Ed* 2023;62:e202216174. DOI
  39. Wang P, You Y, Yin Y, Guo Y. Layered oxide cathodes for sodium-ion batteries: phase transition, air stability, and performance. *Adv Energy Mater* 2018;8:1701912. DOI
  40. Xiao Y, Wang P, Yin Y, et al. A layered-tunnel intergrowth structure for high-performance sodium-ion oxide cathode. *Adv Energy Mater* 2018;8:1800492. DOI
  41. Zhao C, Ding F, Lu Y, Chen L, Hu YS. High-entropy layered oxide cathodes for sodium-ion batteries. *Angew Chem Int Ed* 2020;59:264-9. DOI
  42. Huang Q, Wang M, Zhang L, et al. Shear-resistant interface of layered oxide cathodes for sodium ion batteries. *Energy Stor Mater* 2022;45:389-98. DOI
  43. Lin C, Dai P, Wang X, et al. P2/O3 biphasic integration promoting the enhancement of structural stability for sodium layered oxide cathode. *Chem Eng J* 2024;480:147964. DOI
  44. Mu J, Cai T, Dong W, Zhou C, Han Z, Huang F. Biphasic high-entropy layered oxide as a stable and high-rate cathode for sodium-ion batteries. *Chem Eng J* 2023;471:144403. DOI
  45. Wang SS, Liu ZM, Gao XW, Wang XC, Chen H, Luo WB. Layer-structured multitransition-metal oxide cathode materials for potassium-ion batteries with long cycling lifespan and superior rate capability. *ACS Appl Mater Interfaces* 2023;15:57165-73. DOI PubMed
  46. Mu J, Gao X, Liu Z, et al. Boosting nitrogen electrocatalytic fixation by three-dimensional  $TiO_{2-x}N_x$  nanowire arrays. *J Energy Chem* 2022;75:293-300. DOI
  47. Wang D, Liu Z, Gao X, Gu Q, Zhao L, Luo W. Massive anionic fluorine substitution two-dimensional  $\delta$ - $MnO_2$  nanosheets for high-performance aqueous zinc-ion battery. *J Energy Stor* 2023;72:108740. DOI
  48. Li J, Mu J, Liu Z, et al. Boosting potassium-based dual ion battery with high energy density and long lifespan by red phosphorous. *J Power Sources* 2023;571:233054. DOI
  49. Han MH, Gonzalo E, Singh G, Rojo T. A comprehensive review of sodium layered oxides: powerful cathodes for Na-ion batteries. *Energy Environ Sci* 2015;8:81-102. DOI
  50. Lin C, Liu H, Kang J, et al. In-situ X-ray studies of high-entropy layered oxide cathode for sodium-ion batteries. *Energy Stor Mater* 2022;51:159-71. DOI
  51. Zhang G, Li J, Fan Y, et al. Suppressed P2-P2' phase transition of Fe/Mn-based layered oxide cathode for high-performance sodium-ion batteries. *Energy Stor Mater* 2022;51:559-67. DOI
  52. Yu Y, Ning D, Li Q, et al. Revealing the anionic redox chemistry in  $O_3$ -type layered oxide cathode for sodium-ion batteries. *Energy Stor Mater* 2021;38:130-40. DOI
  53. Zhong L, Qiu X, Yang S, Sun S, Chen L, Zhang W. Supermolecule-regulated synthesis strategy of general biomass-derived highly nitrogen-doped carbons toward potassium-ion hybrid capacitors with enhanced performances. *Energy Stor Mater* 2023;61:102887. DOI
  54. Shi C, Wang L, Chen X, et al. Challenges of layer-structured cathodes for sodium-ion batteries. *Nanoscale Horiz* 2022;7:338-51. DOI
  55. Katcho NA, Carrasco J, Saurel D, et al. Origins of bistability and Na ion mobility difference in P2- and O3- $Na_{2/3}Fe_{2/3}Mn_{1/3}O_2$  cathode polymorphs. *Adv Energy Mater* 2017;7:1601477. DOI
  56. Lee E, Lu J, Ren Y, et al. Layered P2/O3 intergrowth cathode: toward high power Na-ion batteries. *Adv Energy Mater* 2014;4:1400458. DOI
  57. Zhao W, Tsuchiya Y, Yabuuchi N. Influence of synthesis conditions on electrochemical properties of P2-type  $Na_{2/3}Fe_{2/3}Mn_{1/3}O_2$  for rechargeable Na batteries. *Small Methods* 2019;3:1800032. DOI
  58. Cao Y, Zhang Q, Wei Y, et al. A water stable, near-zero-strain  $O_3$ -layered titanium-based anode for long cycle sodium-ion battery. *Adv Funct Mater* 2020;30:1907023. DOI
  59. Yang L, del Amo JML, Shadik Z, et al. A Co- and Ni-Free P2/O3 biphasic lithium stabilized layered oxide for sodium-ion batteries and its cycling behavior. *Adv Funct Mater* 2020;30:2003364. DOI

60. Zhao C, Avdeev M, Chen L, Hu YS. An O<sub>3</sub>-type oxide with low sodium content as the phase-transition-free anode for sodium-ion batteries. *Angew Chem Int Ed* 2018;57:7056-60. DOI PubMed
61. Zhu YF, Xiao Y, Hua WB, et al. Manipulating layered P2@P3 integrated spinel structure evolution for high-performance sodium-ion batteries. *Angew Chem Int Ed* 2020;59:9299-304. DOI
62. Liu Z, Zhou C, Liu J, Yang L, Liu J, Zhu M. Phase tuning of P2/O3-type layered oxide cathode for sodium ion batteries via a simple Li/F co-doping route. *Chem Eng J* 2022;431:134273. DOI
63. Maughan PA, Naden AB, Irvine JTS, Armstrong AR. Manipulating O3/P2 phase ratio in bi-phasic sodium layered oxides via ionic radius control. *Commun Mater* 2023;4:6. DOI
64. Li R, Liu Y, Wang Z, Li J. A P2/O3 biphasic cathode material with highly reversibility synthesized by Sn-substitution for Na-ion batteries. *Electrochim Acta* 2019;318:14-22. DOI
65. Huang J, Li W, Ye D, Xu L, Wu W, Wu X. Designing ultrastable P2/O3-type layered oxides for sodium ion batteries by regulating Na distribution and oxygen redox chemistry. *J Energy Chem* 2024;94:466-76. DOI
66. Zhang L, Guan C, Zheng J, et al. Rational design of intergrowth P2/O3 biphasic layered structure with reversible anionic redox chemistry and structural evolution for Na-ions batteries. *Sci Bull* 2023;68:180-91. DOI
67. Sharma N, Bahri OKA, Han MH, Gonzalo E, Pramudita JC, Rojo T. Comparison of the structural evolution of the O3 and P2 phases of Na<sub>2/3</sub>Fe<sub>2/3</sub>Mn<sub>1/3</sub>O<sub>2</sub> during electrochemical cycling. *Electrochim Acta* 2016;203:189-97. DOI
68. Xu G, Amine R, Xu Y, et al. Insights into the structural effects of layered cathode materials for high voltage sodium-ion batteries. *Energy Environ Sci* 2017;10:1677-93. DOI
69. Zhou D, Huang W, Lv X, Zhao F. A novel P2/O3 biphasic Na<sub>0.67</sub>Fe<sub>0.425</sub>Mn<sub>0.425</sub>Mg<sub>0.15</sub>O<sub>2</sub> as cathode for high-performance sodium-ion batteries. *J Power Sources* 2019;421:147-55. DOI
70. Zhao J, Zhang X, Wang J, Yang X, Deng J, Wang Y. P2-type Na<sub>0.59</sub>Co<sub>0.20</sub>Mn<sub>0.77</sub>Mo<sub>0.03</sub>O<sub>2</sub> cathode with excellent cycle stability for sodium-ion batteries. *J Solid State Electrochem* 2020;24:1349-61. DOI
71. Bianchini M, Wang J, Clément RJ, et al. The interplay between thermodynamics and kinetics in the solid-state synthesis of layered oxides. *Nat Mater* 2020;19:1088-95. DOI
72. Wang JE, Kim H, Jung YH, Kim DK, Kim DJ. Designing high energy sodium-ion battery cathodes by utilizing P2/O3 biphasic structure and lithium honeycomb ordering. *Small* 2021;17:e2100146. DOI
73. Guo S, Liu P, Yu H, et al. A layered P2- and O3-type composite as a high-energy cathode for rechargeable sodium-ion batteries. *Angew Chem Int Ed* 2015;54:5894-9. DOI
74. Qi X, Liu L, Song N, et al. Design and comparative study of O3/P2 hybrid structures for room temperature sodium-ion batteries. *ACS Appl Mater Interfaces* 2017;9:40215-23. DOI
75. Zhou D, Zeng C, Ling D, et al. Sustainable alternative cathodes of sodium-ion batteries using hybrid P2/O3 phase Na<sub>0.67</sub>Fe<sub>0.5</sub>Mn<sub>0.5-x</sub>Mg<sub>x</sub>O<sub>2</sub>. *J Alloys Compd* 2023;931:167567. DOI
76. Zhang P, Zhang G, Liu Y, et al. Constructing P2/O3 biphasic structure of Fe/Mn-based layered oxide cathode for high-performance sodium-ion batteries. *J Colloid Interface Sci* 2024;654:1405-16. DOI
77. Wang K, Wu Z, Melinte G, et al. Preparation of intergrown P/O-type biphasic layered oxides as high-performance cathodes for sodium ion batteries. *J Mater Chem A* 2021;9:13151-60. DOI
78. Hong J, Xiao S, Deng L, Lan T, He G. Li-free P2/O3 biphasic Na<sub>0.73</sub>Ni<sub>0.4</sub>Mn<sub>0.4</sub>Ti<sub>0.2</sub>O<sub>2</sub> as a cathode material for sodium-ion batteries. *Ionics* 2020;26:3911-7. DOI
79. Xu W, Gao X, Zhou Y, Zou G, Hou H, Ji X. Sodium de-insertion processes in single Na<sub>x</sub>TMO<sub>2</sub> particles studied by an electrochemical collision method: O3 phases versus P2 phases. *Electrochem Commun* 2021;125:107000. DOI
80. Zhou P, Che Z, Liu J, et al. High-entropy P2/O3 biphasic cathode materials for wide-temperature rechargeable sodium-ion batteries. *Energy Stor Mater* 2023;57:618-27. DOI
81. Chen C, Huang W, Li Y, et al. P2/O3 biphasic Fe/Mn-based layered oxide cathode with ultrahigh capacity and great cyclability for sodium ion batteries. *Nano Energy* 2021;90:106504. DOI
82. Huang Q, Liu J, Xu S, et al. Roles of coherent interfaces on electrochemical performance of sodium layered oxide cathodes. *Chem Mater* 2018;30:4728-37. DOI
83. Yu L, Cheng Z, Xu K, et al. Interlocking biphasic chemistry for high-voltage P2/O3 sodium layered oxide cathode. *Energy Stor Mater* 2022;50:730-9. DOI
84. Hu B, Geng F, Zhao C, et al. Deciphering the origin of high electrochemical performance in a novel Ti-substituted P2/O3 biphasic cathode for sodium-ion batteries. *ACS Appl Mater Interfaces* 2020;12:41485-94. DOI
85. Gao G, Tie D, Ma H, et al. Interface-rich mixed P2 + T phase Na<sub>x</sub>Co<sub>0.1</sub>Mn<sub>0.9</sub>O<sub>2</sub> (0.44 ≤ x ≤ 0.7) toward fast and high capacity sodium storage. *J Mater Chem A* 2018;6:6675-84. DOI
86. Zhang Z, Liu Y, Liu Z, et al. Dual-strategy of Cu-doping and O3 biphasic structure enables Fe/Mn-based layered oxide for high-performance sodium-ion batteries cathode. *J Power Sources* 2023;567:232930. DOI
87. Feng J, Fang D, Yang Z, et al. A novel P2/O3 composite cathode toward synergistic electrochemical optimization for sodium ion batteries. *J Power Sources* 2023;553:232292. DOI
88. Wang P, You Y, Yin Y, et al. Suppressing the P2-O2 Phase Transition of Na<sub>0.67</sub>Mn<sub>0.67</sub>Ni<sub>0.33</sub>O<sub>2</sub> by magnesium substitution for improved sodium-ion batteries. *Angew Chem Int Ed* 2016;128:7571-5. DOI
89. Wang QC, Meng JK, Yue XY, et al. Tuning P2-structured cathode material by Na-site Mg substitution for Na-ion batteries. *J Am*

- Chem Soc* 2019;141:840-8. DOI
90. Tao S, Zhou W, Wu D, et al. Insights into the  $Ti^{4+}$  doping in P2-type  $Na_{0.67}Ni_{0.33}Mn_{0.52}Ti_{0.15}O_2$  for enhanced performance of sodium-ion batteries. *J Mater Sci Technol* 2021;74:230-6. DOI
  91. Wang JZ, Teng YX, Su GQ, Bao S, Lu JL. A dual-modification strategy for P2-type layered oxide via bulk Mg/Ti co-substitution and MgO surface coating for sodium ion batteries. *J Colloid Interface Sci* 2022;608:3013-21. DOI
  92. Kaliyappan K, Liu J, Lushington A, Li R, Sun X. Highly stable  $Na_{2/3}(Mn_{0.54}Ni_{0.13}Co_{0.13})O_2$  cathode modified by atomic layer deposition for sodium-ion batteries. *ChemSusChem* 2015;8:2537-43. DOI
  93. Liu Y, Fang X, Zhang A, et al. Layered P2- $Na_{2/3}[Ni_{1/3}Mn_{2/3}]O_2$  as high-voltage cathode for sodium-ion batteries: the capacity decay mechanism and  $Al_2O_3$  surface modification. *Nano Energy* 2016;27:27-34. DOI
  94. Li N, Ren J, Dang R, et al. Suppressing phase transition and improving electrochemical performances of O3- $NaNi_{1/3}Mn_{1/3}Fe_{1/3}O_2$  through ionic conductive  $Na_2SiO_3$  coating. *J Power Sources* 2019;429:38-45. DOI
  95. Xue L, Bao S, Yan L, Zhang Y, Lu J, Yin Y. MgO-coated layered cathode oxide with enhanced stability for sodium-ion batteries. *Front Energy Res* 2022;10:847818. DOI
  96. Hwang J, Myung S, Choi JU, Yoon CS, Yashiro H, Sun Y. Resolving the degradation pathways of the O3-type layered oxide cathode surface through the nano-scale aluminum oxide coating for high-energy density sodium-ion batteries. *J Mater Chem A* 2017;5:23671-80. DOI
  97. Yang J, Lim J, Park M, et al. Thermally activated P2-O3 mixed layered cathodes toward synergistic electrochemical enhancement for Na ion batteries. *Adv Energy Mater* 2021;11:2102444. DOI
  98. Zuo W, Qiu J, Liu X, et al. Highly-stable P2- $Na_{0.67}MnO_2$  electrode enabled by lattice tailoring and surface engineering. *Energy Stor Mater* 2020;26:503-12. DOI
  99. Xiao Y, Wang HR, Hu HY, et al. Formulating high-rate and long-cycle heterostructured layered oxide cathodes by local chemistry and orbital hybridization modulation for sodium-ion batteries. *Adv Mater* 2022;34:e2202695. DOI
  100. Jiang N, Liu Q, Wang J, et al. Tailoring P2/P3 biphases of layered  $Na_xMnO_2$  by Co substitution for high-performance sodium-ion battery. *Small* 2021;17:e2007103. DOI